SCIENCE CHINA
Life Sciences

• RESEARCH PAPER •

December 2014 Vol.57 No.12: 1191–1196
doi: 10.1007/s11427-014-4731-1

An *in vitro* and finite element study of load redistribution in the midfoot

NIU WenXin[1,2,3], TANG TingTing[4], ZHANG Ming[2], JIANG ChengHua[5*] & FAN YuBo[3*]

[1]*Tongji Hospital, Tongji University School of Medicine, Shanghai 200092, China;*
[2]*Interdisciplinary Division of Biomedical Engineering, Faculty of Engineering, The Hong Kong Polytechnic University, Hong Kong, China;*
[3]*Laboratory for Biomechanics and Mechanobiology of Ministry of Education, School of Biological Science and Medical Engineering, Beihang University, Beijing 100191, China*
[4]*Shanghai Key Laboratory of Orthopaedic Implants, Shanghai 200011, China;*
[5]*Department of Disaster and Emergency Medicine, Eastern Hospital, Tongji University School of Medicine, Shanghai 200120, China*

Received February 13, 2014; accepted April 17, 2014; published online September 22, 2014

A good knowledge of midfoot biomechanics is important in understanding the biomechanics of the entire foot, but it has never been investigated thoroughly in the literature. This study carried out *in vitro* experiments and finite element analysis to investigate the midfoot biomechanics. A foot-ankle finite element model simulating the mid-stance phase of the normal gait was developed and the model validated in *in vitro* experimental tests. Experiments used seven *in vitro* samples of fresh human cadavers. The simulation found that the first principal stress peaks of all midfoot bones occurred at the navicular bone and that the tensile force of the spring ligament was greater than that of any other ligament. The experiments showed that the longitudinal strain acting on the medial cuneiform bone was –26.2±10.8 μ-strain, and the navicular strain was –240.0±169.1 μ-strain along the longitudinal direction and 65.1±25.8 μ-strain along the transverse direction. The anatomical position and the spring ligament both result in higher shear stress in the navicular bone. The load from the ankle joint to five branches of the forefoot is redistributed among the cuneiforms and cuboid bones. Further studies on the mechanism of loading redistribution will be helpful in understanding the biomechanics of the entire foot.

finite element analysis, foot arch, biomechanics, cadaveric experiment, midfoot

Citation: Niu WX, Tang TT, Zhang M, Jiang CH, Fan YB. An *in vitro* and finite element study of load redistribution in the midfoot. Sci China Life Sci, 2014, 57: 1191−1196, doi: 10.1007/s11427-014-4731-1

The human foot can be divided into three parts from the posterior to the anterior: the rearfoot (hindfoot), midfoot and forefoot. Many acute traumas, stress fractures, chronic diseases, deformiies and instability problems associated with biomechanics occur in the rearfoot or forefoot region [1–7]. During static standing or motion, the rearfoot and forefoot directly contact the ground and their biomechanics has been thoroughly researched. [5–7]. Two recent experiments showed that the rearfoot and forefoot support about 80%–90% of body weight while standing [5,6].

The midfoot includes the cuboid (Cu), navicular (Na), medial (C1), intermediate (C2) and lateral cuneiform (C3) bones, and surrounding soft tissues. Relatively few studies have focused on the biomechanics of the midfoot [8]. Injuries of the midfoot are relatively rare, but they are subtle and can lead to long-term morbidity if missed [9,10]. In the midfoot, injuries mainly occur to the Na bone and not to the four other bones [10].

The foot has both longitudinal and transverse arches. Scientists have deeply and widely investigated the biomechanical and clinical significances of the medial and lateral

*Corresponding author (email: jch@tongji.edu.cn; yubofan@buaa.edu.cn)

longitudinal arches [11]. Nevertheless, there is very limited knowledge on how the load is distributed and how the mechanical information is split between two longitudinal arches. The midfoot is the only connection of the two longitudinal arches after they bifurcate at the heel and before they re-diverge from each other at five metatarsal (MT) branches. The midfoot may play a vital role in the loading change between the two longitudinal arches, but nobody knows how the biomechanical function acts during stance.

The finite element method (FEM) is a powerful technique that reconstructs strain, stress, and deformation using a numerical model. It has been applied in biomechanics since the 1970s. Currently, the technological development of both hardware and software supports solutions with sophisticated models or algorithms [4,7,11–15]. The present study carried out finite element analysis and *in vitro* experiments to investigate the biomechanical response of midfoot bones during the stance phase of normal gait.

1 Materials and methods

1.1 Finite element modeling

A male adult with no foot pathology or trauma history was selected. For preparation of a three-dimensional FE model, foot-ankle-shank complex data were obtained from computer tomography scans at 0.625-mm intervals in the unloaded neutral foot position along the transverse plane. To reconstruct the geometries of bones and the skin surface, the scanned images were processed with MIMICS 12.0 software. Solid models for each bone and the whole foot surface were created from boundary surfaces with Geomagic Studio 9 software. All solid models were then imported and assembled in ANSYS 11.0 (ANSYS Inc., USA) for FE meshing and analysis.

The FE model consisted of the distal tibia and fibula and 28 foot bones: the talus, calcaneus, Na, C1, C2, C3, Cu, five MTs, 14 phalanges and two sesamoid bones. As shown in Figure 1, all bones were embedded in a volume of encapsulated bulk soft tissue. All phalanges in each ray were connected together. The interactions among articulated bones were defined as contacting elastic bodies to allow relative bone movement. Except for the ligaments around phalanges, all ligaments and plantar fasciae were modeled with tension-only link elements. Bones and soft-tissue structures were all meshed with quadratic tetrahedral elements, while the articular cartilages were modeled extracting the corresponding bone surface elements.

The material properties of all tissues were assigned according to previous simulations or experimental reports [2,12–14,16–21]. Bones and cartilages were idealized as being homogeneous, isotropic, and linearly elastic. The Young's modulus and Poisson ratio of bones were chosen as 7.3 GPa and 0.3 respectively [2,16–18]. According to experimental measurements, the ankle joint and inter-foot joints had different material properties and cartilages thicknesses. Table 1 summarizes all the above-mentioned data and references.

Siegler et al. [20] reported the tensile mechanical properties of the collateral ligaments of the ankle joint. The Young's modulus of tibiofibular interosseous membrane was estimated according to the ultimate tensile stress and strain at rupture [21]. The Young's moduli were selected as 260 MPa for other inter-foot ligaments and 350 MPa for the plantar fascia [12]. The cross-section area (CSA) of the plantar fascia was calculated according to the thickness measurement measured by Pavan et al. [22]. Mkandawire et al. [23] measured and established a morphometric spectrum of CSAs for the foot and ankle ligaments. In the case that the ligaments were neither included in this spectrum nor measured by Siegler et al. [20], CSAs were selected according to neighboring or analogical ligaments. The encapsulated soft tissue of the FE model was defined as being hyperelastic and was described by the Mooney-Rivlin reduced polynomial model [24].

1.2 Finite element analysis

The stance phase accounts for 60% of the normal gait cycle. The foot is loaded mainly in this phase because it is free from body weight loading in the swinging phase. The stance phase is divided into five sub-phases: heel strike, foot flat, mid-stance, heel off and toe off. This study simulated the mid-stance phase because the FE model was constructed in the neutral position, the most representative for evaluating gait biomechanics.

The mid-stance phase occurs when the swinging limb just passes the stance limb. During this time, the stance limb becomes almost vertical and provides single-limb support, as the other limb freely swings forward. The dorsiflexors

Figure 1 Finite element of the foot-ankle complex. A, The complete model. B, Element meshing of bones and ligaments. C, Perspective line drawing of the model.

are inactive and plantar flexors eccentrically contract to control the rate at which the swinging limb moves past the stance foot. During the stance phase, the vertical ground reaction force is approximately the body weight [25]. Therefore, in the simulation, the plantar surface was restrained with a rigid plate in the vertical direction, and a vertical loading was distributed on the tibia sections. Considering the force of the Achilles tendon, the resultant force should be equal to the body weight of 700 N.

The triceps surae muscle has one major long-duration phase of activity throughout the stance phase. The forces are loaded on the posterior part of the calcaneal through the Achilles tendon [25]. Lin et al. [26] reported the muscle force exerted by the triceps surae. The data, provided with curves by Lin et al. [26], were normalized to the body weight and re-computed as Achilles tendon forces of 700 N for the mid-stance phase in the preset study. This value is identical to that calculated by Cheung & Zhang [14] using another method.

The simulation calculated stresses and strains of the midfoot bones, and the ligament forces. This research used the first and third principal stresses, because they represent the maximum tensile and maximum compressive stresses in the direction of principal stress, respectively. Force and pressure were also computed at various joints of the midfoot. The application of pressure sensitive films has demonstrated the possibility of investigating the articulating surface loads of the tibiotalar [27], subtalar [28–30], talonavicular [29], calcaneocuboid [29,31], tarsometatarsal [32] and metatarsophalangeal joints [33]. Although Ward & Soames [34] measured the contact patterns at the intercuneiform, cuneonavicular, cuneocuboid, and cubonavicular joints by injecting colored dyes, they obtained only data for the contact areas and not pressures data of these joints. It is impossible to measure all articulations with films because the gaps of some articulations are too small to insert the films. This study also analyzed the stress distributed on the articular surfaces between C1 through C3 and Cu.

1.3 *In vitro* experiment

Seven fresh human cadaveric foot-shank complex specimens were tested. Specimens were radiographed to exclud the osseous pathology of preexisting disease or trauma. The specimens were amputated at the mid-tibia level. Skin and muscles of legs were stripped from 5 cm above ankle joints, while the ankle ligaments and Achilles tendons were left intact. The Achilles tendons were sutured using the Krackow technique and the suture silks were loaded with a standard weight of 70 kg through a pulley.

The tibia shafts were fixed to a material testing machine. A vertical load of 700 N with loading rate of 2 mm min^{-1} was applied in 10 cycles. Each specimen was treated in advance with 10-cycles of preconditioning before the formal trial, to account for viscoelastic properties. The output strain was obtained once the specimen was stable.

Strain gauges were used to measure the surface strains of Na and C1. Figure 2 shows that the strains of Na were measured along longitudinal and transverse directions. The strain of C1 was only measured along the longitudinal direction. Before installing the strain gauges, the bone was dried with anhydrous alcohol and degreased with acetone. A temperature compensated gauge was installed to a fibula section of the same specimen for each trail.

2 Results

2.1 Principal stress of finite element analysis

Figure 3 shows the von Mises stress peaks and the first and third principal stresses of midfoot bones. The concentrations of three stresses of Na all occurred at the insertion point of

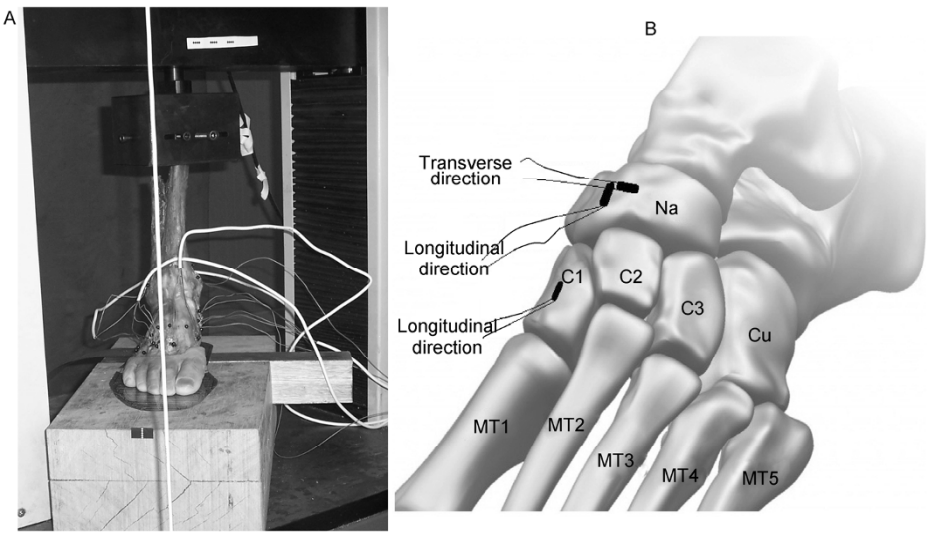

Figure 2 *In vitro* experiment on foot biomechanics. A, Laboratory scene. B, Schematic diagram of the positions and directions of strain gages.

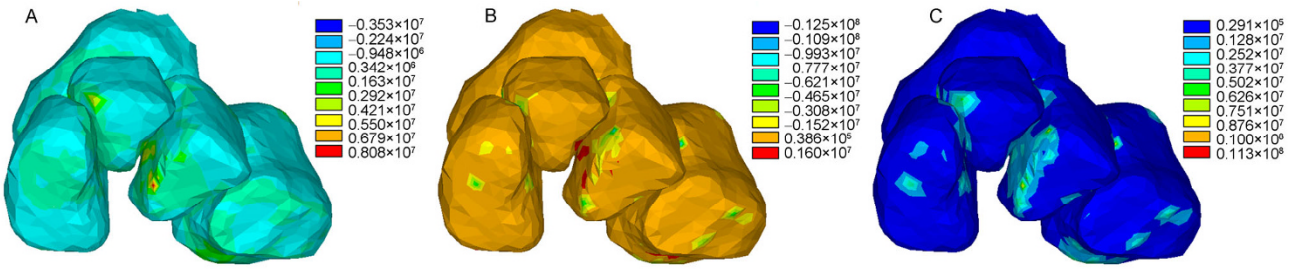

Figure 3 Stress results of the midfoot bones. A, First principal stress. B, Third principal stress. C, von Mises stress.

the spring ligament, and the absolute third principal stress concentration also occurred at the articular surfaces of the talonavicular and cuneonavicular joints.

The von Mises stress peaks were higher for Na, C3, and C2 than for C1 and Cu. Among all midfoot bones, Na had the highest peak of first principal stress, but the lowest peak absolute of third principal stress. The peak of first principal stress for the other four bones decreased in the order: C3>C2>Cu>C1. The peak absolute of third principal stress for the above-mentioned four bones ranged from 9.79 to 11.2 MPa.

The von Mises peaks and the first and third stresses of C1 were all concentrated at the first intercuneiform articular surface. The von Mises stress and the first principal stress concentration of C2 occurred at the second intercuneiform articular surface. Moreover, the absolute third principal stress concentration occurred between the cuneonavicular and the C2 and C3 joints. All stress peaks of C3 were mainly distributed on the cuneocuboid articular surface. All stress peaks of Cu were mainly distributed on the cuneocuboid articular surface and at the insertion point of the cuneocuboid ligament.

The spring ligament, short plantar ligament and plantar cuneocuboid ligament had stronger tensile forces of 82, 49 and 27 N respectively. Most other ligaments within the midfoot, especially the dorsal ligaments, maintained relax and produced less tensile force.

2.2 Experimental measurements of strain

The *in vitro* experiments revealed that C1 produced compressive strain of –26.2±10.8 μ-strain along the longitudinal direction. Na produced compressive strain of –240.0±169.1 μ-strain along the longitudinal direction, and tensile strain of 65.1±25.8 μ-strain along the transverse direction.

3 Discussion

FE analysis carried out by Cheung et al. [12], simulating normal standing with two legs, calculated von Mises stress peaks of 1.47, 0.63, 1.42, 2.22, and 1.58 MPa respectively for Na, C1, C2, C3 and Cu. These computations could be considered reference values for this research, although bearing in mind that the values will be higher in the case of standing on a single leg. Thus, considering the different loading conditions and individual variations, the differences were understandable and acceptable.

The von Mises stress peaks were larger for Na and C3 than for C1, C2, and Cu, although the differences were very small. This did not provide relevant information to allow more accurate injury prediction. The absolute third principal stress peak was significantly lower for Na than for other bones. Moreover, the first principal stress peak was highest for Na among all midfoot bones. Therefore, the greater von Mises stress for Na was more related to the first principal stress than the third principal stress. The tensile strength of long cancellous bone is only about 70% of the compressive strength [35,36]. This means that the cancellous bone is more likely to be damaged by tensile stress than by compressive stress. This feature explains why Na faces greater fracture risk than other bones under similar or even less von Mises stress, according to the results obtained in this study and the study of Cheung et al. [12].

The *in vitro* experiments revealed a great difference in strain measurements between Na and C1 bones. The strain gauge could only give local strain information, and the measurement greatly depended on the gauge size, position, and direction. Thus, the experiments could not absolutely demonstrate that there was greater strain for Na than for C1. However, tests showed that both bones were compressed along the longitudinal direction and Na was stretched in the transverse direction. Na is located between the talus and C1, C2 and C3 and articulates with them via the talonavicular and cuneonavicular joints. This circumstance of unidirectional compression provides tensile strain in the transverse direction. The wide articular surfaces promote tensile strain extending thorough the narrow transverse strap. This may contribute to the sensitivity of Na to stress fracture under cyclic loading.

Bones C1 through C3 have similar stress amplitudes and distributions. They all are articulated with Na upstream and with MTs downstream. The loading from Na to MTs is allocated and regulated trough C1, C2 and C3. If one of the cuneiforms carries markedly greater or smaller loading than the other cuneiforms, the load can be redistributed among

the bones. This mechanism protects cuneiforms from high stress and potential injury; however, this process at the cuneonavicular joint deteriorates the biomechanical environment of Na. The three bearing regions work as a bending moment producing more complex tensile or shear stress on the bone that can damage Na during load regulation.

The FE simulation also showed that the higher stresses of Na were largely due to spring ligament. The analysis demonstrated the important effect of spring ligament on the foot structure. Cheung et al. [13] found that the force loaded on the spring ligament was 50 N for a two–foot balanced landing. The present study revealed a force of 82 N during a single–foot stance phase.

The concentrations of principal stress were mainly located on the articular surfaces of intercuneiform and cuneocuboid joints. Previous biomechanical studies focused more on the cuneonavicular, calcaneocuboid, and tarsometatarsal joints in the longitudinal direction, because they transfer the loading from the ankle to the forefoot. However, the loading transfer mechanism in the transverse direction is also important.

Compared with the medial sides, both C2 and C3 had greater stress peaks on the lateral articular surfaces. These two bones were also subject to greater stresses than C1 and Cu. Figure 4 shows that the loading should be transferred from C2 to C1 and from C3 to Cu. Like a stream, the loading passes from a higher to lower stress region, and from the midstream to the brinks. The mechanism is always reflected as the abduction of four bones to different degrees. Compared with the lateral longitudinal column, the medial column is more efficient in transferring the load from the ankle joint to the forefoot. The loading re-distribution communicates the force stream between two longitudinal arches, and compensates the deficit of the lateral column.

The force transfer within the midfoot makes C1, C2, C3 and Cu concordant in the loading bearing. Force transfer can effectively reduce higher stress on a certain bone or certain location, and greatly influences injury risks in the midfoot. Moreover, the cross-sections of C1, C2, C3, and Cu in the sagittal plane were mainly filled with osseous tissue. Therefore, as the stiffest section, the synergetic four bones can avoid injuries. The mechanism of load re-distribution mechanism within the midfoot also balances the load on the forefoot; this affect the stress and even injury risks of the forefoot tissues.

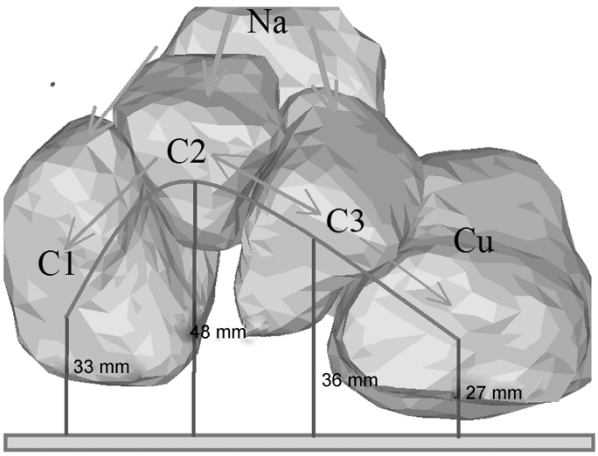

Figure 4 Load re-distribution among cuneiform and cuboid bones.

In conclusion, the stress fracture of the midfoot generally occurs at the Na mainly because of tensile stress in the transverse direction. The anatomical position and spring ligament are both important to the biomechanical environment of Na. The load from the ankle joint to five branches of the forefoot is redistributed among C1, C2, C3 and Cu. Further studies on the mechanism of the load redistribution will be helpful in understanding the biomechanics of the entire foot.

This work was supported by the National Natural Science Foundation of China (11302154, 11272273), China Postdoctoral Science Foundation (2013M530211), Opening Project of Shanghai Key Laboratory of Orthopaedic Implants (KFKT2013002) and Fundamental Research Funds for the Central Universities.

1 Snedeker JG, Wirth SH, Espinosa N. Biomechanics of the normal and arthritic ankle joint. Foot Ankle Clin, 2012, 17: 517–528
2 Collan L, Kankare JA, Mattila K. The biomechanics of the first bone in hallux valgus: A preliminary study utilizing a weight bearing extremity CT. Foot Ankle Surg, 2013, 19: 155–161
3 Moshirfar A, Campbell JT, Molloy S, Jasper LE, Belkoff SM. Fifth metatarsal tuberosity fracture fixation: a biomechanical study. Foot Ankle Int, 2003, 24: 630–633
4 Ni M, Weng XH, Mei J, Niu WX. Primary stability of absorbable screw fixation for intra-articular calcaneal fractures: A finite element analysis. J Med Biol Eng, advance online publication 26 Mar. 2014; doi: 10.5405/jmbe.1624
5 Niu WX, Yao J, Chu ZW, Jiang CH, Zhang M, Fan YB. Effects of ankle eversion, limb laterality and ankle stabilizers on transient postural stability during unipedal standing. J Med Biol Eng, advance online publication 4 Dec. 2013; doi: 10.5405/jmbe.1675.
6 Niu W, Chu Z, Yao J, Zhang M, Fan Y, Zhao Q. Effects of laterality, ankle inversion and stabilizers on the plantar pressure distribution during unipedal standing. J Mech Med Biol, 2012, 12: 1250055
7 Yu J, Cheung JTM, Wong DWC, Cong Y, Zhang M. Biomechanical simulation of high-heel shoe donning and walking. J Biomech, 2013, 46: 2067–2074
8 Benirschke SK, Meinberg E, Anderson SA, Jones CB, Cole PA. Fractures and dislocations of the midffot: Lisfrac and Chopart injuries. J Bone Joint Surg Am, 2012, 18: 1325–1337
9 Pearce CJ, Calder JD. Surgical anatomy of the midfoot. Knee Surg Sports Traumatol Arthrosc, 2010, 18: 581–586
10 Makwana NK, van Lifefland MR. Injuries of the midfoot. Current Orthopaedics, 2005, 19: 231–242
11 Liang J, Yang Y, Yu G, Niu W, Wang Y. Deformation and stress distribution of the human foot after plantar ligament release: a cadaveric study and finite element analysis. Sci China Life Sci, 2011, 54: 267–271
12 Cheung JTM, Zhang M, Leung AKL, Fan YB. Three-dimensional finite element analysis of the foot during standing: a material sensitivity study. J Biomech, 2005, 38: 1045–1054
13 Cheung JTM, An KN, Zhang M. Consequences of partial and total plantar fascia release: a finite element study. Foot Ankle Int, 2006, 27: 125–132

14 Cheung JTM, Zhang M. Parametric design of pressure-relieving foot orthosis using statistics-based finite element method. Med Eng Phys, 2008, 30: 269–277
15 Huang RH, Li XP, Rong QG. Control mechanism for the upper airway collapse in patients with obstructive sleep apnea syndrome: a finite element study. Sci China Life Sci, 2013, 56: 366–372
16 Athansiou KA, Niederauer GG, Schenck RC Jr. Biomechanical topography of human ankle cartilage. Ann Biomed Eng, 1995, 23: 697–704
17 Athansiou KA, Fleischli JG, Bosma J, Laughlin TJ, Zhu CF, Agrawal CM, Lavery LA. Effects of diabetes mellitus on the biomechanical properties of human ankle cartilage. Clin Orthop Relat Res, 1999, 368: 182–189
18 Athansiou KA, Liu GT, Lavery LA, Lanctot DR, Schenck RC Jr. Biomechanical topography of human articular cartilage in the first metatarsophalangeal joint. Clin Orthop Relat Res, 1998, 348: 269–291
19 Liu GT, Lavery LA, Schenck RC Jr, Lanctot DR, Zhu CF, Athansiou KA. Human articular cartilage biomechanics of the second metatarsal intermediate cuneiform joint. J Foot Ankle Surg, 1997, 36: 367–374
20 Siegler S, Block J, Schneck CD. The mechanical characteristics of the collateral ligaments of the human ankle joint. Foot Ankle, 1988, 8: 234–242
21 Minns RJ, Hunter JA. The mechanical and structural characteristics of the tibio-fibular interosseous membrane. Acta Orthop Scand, 1976, 47: 236–240
22 Pavan PG, Stecco C, Darwish S, Natali AN, De Caro R. Investigation of the mechanical properties of the plantar aponeurosis. Surg Radiol Anat, 2011, 33: 905–911
23 Mkandawire C, Ledoux WR, Sangeorzan BJ, Ching RP. Foot and ankle ligament morphometry. J Rehabil Res Dev, 2005, 42: 809–820
24 Spears IR, Miller-Young JE, Waters M, Rome K. The effect of loading conditions on stress in the barefooted heel pad. Med Sci Sports Exerc, 2005, 37: 1030–1065
25 Rodgers MM. Dynamic biomechanics of the normal foot and ankle during walking and running. Phys Ther, 1988, 68: 1822–1830
26 Lin YC, Dorn TW, Schache AG, Pandy MG. Comparison of different methods for estimating muscle forces in human movement. Proc Inst Mech Eng H, 2012, 226: 103–112
27 Martinelli N, Marinozzi A, Schulze M, Denaro V, Evers J, Bianchi A, Rosenbaum D. Effect of subtalar arthroereisis on the tibiotalar contact characteristics in a cadaveric flatfoot model. J Biomech, 2012, 45: 1745–1748
28 Wang CL, Cheng CK, Chen CW, Lu CM, Hang YS, Liu TK. Contact areas and pressure distributions in the subtalar joint. J Biomech, 1995, 28: 269–279
29 Jung HG, Parks BG, Nguyen A, Schon LC. Effect of tibiotalar joint arthrodesis on adjacent tarsal joint pressure in a cadaver model. Foot Ankle Int, 2007, 28: 103–108
30 Thomas JL, Moeini R, Doileau R. The effect on subtalar contact and pressure following talonavicular and midtarsal joint arthrodesis. J Foot Ankle Surg, 2000, 39: 78–88
31 Momberger N, Morgan JM, Bachus KN, West JR. Calcaneocuboid joint pressure after lateral column lengthening in a cadaveric planovalgus deformity model. Foot Ankle Int, 2000, 21: 730–735
32 Lakin RC, Degnore LT, Pienkowski D. Contact mechanics of normal tarsometatarsal joints. J Bone Joint Surg Am, 2001, 83: 520–528
33 Schneider T, Dabirrahmani D, Gillies RM, Appleyard RC. Biomechanical comparison of metatarsal head designs in first metatarsophalangeal joint arthroplasty. Foot Ankle Int, 2013, 34: 881–889
34 Ward KN, Soames RW. Contact patterns at the tarsal joints. Clin Biomech (Bristol, Avon), 1997, 12: 496–507
35 Keaveny TM, Wachtel EF, Ford CM, Hayes WC. Differences between the tensile and compressive strengths of bovine tibial trabecular depend on modulus. J Biomech, 1994, 27: 1137–1146
36 Bayrakrar HH, Morgan EF, Niebur GL, Morris GE, Wong EK, Keaveny TM. Comparison of the elastic and yield properties of human femoral trabecular and cortical bone tissue. J Biomech, 2004, 37: 27–35